Modeling of Seeded Reflective Modulators for DWDM Systems

Joon-Young Kim, Sang-Rok Moon, Sang-Hwa Yoo, and Chang-Hee Lee, *Fellow, IEEE*

***Abstract*—We propose a theoretical model of reflective modulators for a seeded dense wavelength-division multiplexing (DWDM) system based on amplified spontaneous emission light. A travelling-wave amplifier model is modified to take into account the finite front-facet reflectivity. The net gain and phase shift are updated at every round trip of the cavity to have complex gain for the injected field. With the proposed model, we calculate side-mode suppression ratio, gain, relative intensity noise suppression as a function of injection power, and wavelength detuning for antireflection-coated Fabry-Perot laser diodes. We also investigate the performance of the seeded DWDM system by using the model. The simulation results match well with the experimental results.**

***Index Terms*—Amplified spontaneous emission (ASE) injection seeding, dense WDM (DWDM) system, impairments, reflective modulator, wavelength-division multiplexing–passive optical network (WDM-PON).**

I. Introduction

THERE has been a significant upsurge in video-centric services, including high-definition (HD) television, three-dimensional (3-D) television, video communications, etc. Moreover, the platform of wireless communication is being merged with that of wired communication. To embrace the recent changes, optical fiber is being substituted for existing copper-based transmission media, providing a much higher bandwidth with extended reach. Among the various methods to realize the fiber-to-the-x (FTTx) deployment, wavelength-division multiplexing–passive optical networks (WDM-PONs) have been regarded as a prime solution due to their unlimited bandwidth, high reliability, high security, easy maintenance, and protocol transparency [1]. However, the universal deployment of WDM-PONs hangs on the realization of a cost-effective and color-free optical source [1]. For this, several methods have been proposed and demonstrated. Among them, the injection seeding method has been considered a strong candidate [2]–[4]. In particular, the injection-seeded WDM-PON employing spectrum-sliced amplified spontaneous emission (ASE) light has come to the forefront due to its easy maintenance, color-free operation, and the viability of giga-bit transmission of each subscriber [4], [5].

Note that a dense wavelength-division multiplexing (DWDM) system including the WDM-PON based on injection seeding technology became an international standard of International Telecommunication Union Telecommunication Standardization Sector (ITU-T). The ITU-T Recommendation G.698.3 specifies optical interfaces of a 1.25 Gb/s x 32 channel system [6]. Seed light from the head end is injected to multiple tail ends. Each tail end is equipped with a reflective modulator, such as a Fabry-Perot laser diode (F-P LD) or a reflective semiconductor optical amplifier (RSOA) to provide color-free or colorless operation.

It has been recognized that the performance of a DWDM system (or DWDM-PON) with ASE seeding is limited by the ASE-ASE beating noise arising from the spectrum slicing of the incoherent light [7]–[9]. In addition, there is a variety of system-related impairments, such as a complex noise evolution and back reflections [10]–[14]. Such limiting factors can be overcome to some degree by the help of noise suppression and amplification with the reflective modulator. Thus, a reflective modulator plays a key role in determining the system performance in terms of total capacity (data rate per channel $\times$ channel counts) and/or transmission distance. To understand the system's physical properties and analyze its performance, a multimode rate equation was utilized [15]. However, the result is not reliable when the injection wavelength is located between lasing modes.

In this paper, we propose a simple theoretical model of the reflective modulator for the seeded DWDM system. A travelling-wave amplifier model was modified to take into account the finite reflectivity of the front facet of the reflective modulator [16]. At every round trip of the cavity, the round-trip net gain and phase shift are updated to include boundary conditions. Using this model, we investigated the amplification and noise suppression with respect to various conditions. Also, we examined the noise evolution via optical link as well as back-reflection-induced penalties. The experimental results match well with the simulation results.

The remainder of this paper is organized as follows. In Section II, we briefly introduce the architecture of the seeded DWDM system. In Section III, we explain the numerical generation of the spectrum-sliced ASE as well as the proposed model of the reflective modulator. Based on the model, in Section IV, we provide the analysis results, such as gain, noise suppression, noise increase, and back reflections.

II. Architecture of Seeded DWDM System

The structure of the seeded DWDM system based on ASE light is shown in Fig. 1. In upstream transmission, ASE light

Manuscript received December 1, 2012; revised March 15, 2013; accepted March 22, 2013. Date of publication April 29, 2013; date of current version May 24, 2013. This work was supported in part by the Korea Communications Commission (KCC), Korea, under the R&D Program supervised by the Korea Communications Agency (KCA).

The authors are with the Department of Electrical Engineering, Korea Advanced Institute of Science and Technology (KAIST), Daejeon 305-701, Korea (e-mail: domizzoo@kaist.ac.kr; msr0193@kaist.ac.kr; yoosh321@kaist.ac.kr; changheelee@kaist.edu).

Color versions of one or more of the figures in this paper are available online at http://ieeexplore.ieee.org.

Digital Object Identifier 10.1109/JSTQE.2013.2255586

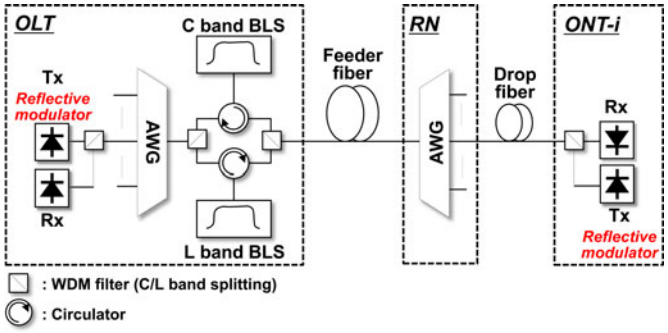

Fig. 1. Architecture of the seeded DWDM system based on ASE light.

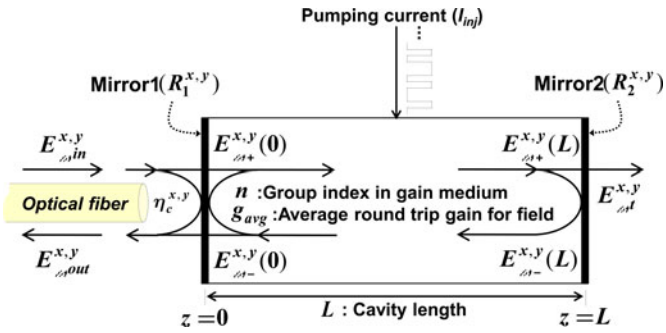

Fig. 2. Schematic drawing of travelling fields inside the reflective modulator.

from the C band broadband light source (BLS) at an optical line terminal (OLT) is delivered to several transmitters at the optical network terminals (ONTs). The optical spectrum of ASE is filtered by the arrayed waveguide grating (AWG) at the remote node (RN). Then, the spectrum-sliced ASE is injected to the reflective modulator that performs modulation, amplification, and noise suppression at the same time. The output light from the reflective modulator is transmitted to the receiver at the OLT in the opposite direction to the seed light.

III. Theoretical Model

A. Spectrum-Sliced ASE

The complex field of ASE light from the BLS is given by

$$\boldsymbol{E}_{\mathrm{ASE}}^{x,y}(\omega) = |\boldsymbol{E}_{\mathrm{ASE}}^{x,y}(\omega)|\, \boldsymbol{e}^{i\phi^{x,y}} \tag{1}$$

where $|\boldsymbol{E}_{\mathrm{ASE}}^{x,y}(\omega)|$ is the constant amplitude in the frequency domain and $\phi^{x,y}$ is a random phase that is uniformly distributed at [0–2π]. The superscripts $\boldsymbol{x}$ and $\boldsymbol{y}$ stand for polarization of the field. For simplicity, we omitted the optical carrier term under a slowly varying envelope approximation. The field of spectrum-sliced ASE can be obtained by multiplying the square root of the AWG transfer function ($H_{\mathrm{AWG}}^{x,y}(\omega)$) as

$$\boldsymbol{E}_{SS\mathrm{ASE}}^{x,y}(\omega) = \boldsymbol{E}_{\mathrm{ASE}}^{x,y}(\omega)\sqrt{\boldsymbol{H}_{\mathrm{AWG}}(\omega)}. \tag{2}$$

The AWG has a passband of a super-Gaussian filter:

$$\boldsymbol{H}_{\mathrm{AWG}}(\omega) = \exp\left[-\ln \mathbf{2}\left(\frac{|\omega|}{\Delta\omega_{\mathrm{AWG}}/\mathbf{2}}\right)^{2n}\right] \tag{3}$$

where $\Delta\omega_{\mathrm{AWG}}$ is the 3 dB bandwidth of the AWG and $\boldsymbol{n}$ is the filter order. The intensity fluctuation induced by the beating between uncorrelated frequency components of the spectrum-sliced ASE can be modeled with the relative intensity noise (RIN). Given that the power spectral density is $\boldsymbol{S}_E(\nu)$, the RIN of the filtered ASE can be calculated as

$$\mathrm{RIN} = \frac{\boldsymbol{S}_E(\nu) * \boldsymbol{S}_E(\nu)}{\boldsymbol{P}_o^2} \tag{4}$$

where $\boldsymbol{P}_o$ is the optical mean power of the spectrum-sliced ASE.

B. Theoretical Model of Reflective Modulator

Fig. 2 shows the simplified structure of the reflective modulator that consists of a gain medium for amplification between two mirrors. We assumed a uniform carrier distribution in the medium. When the input field $\boldsymbol{E}_{\omega,in}^{x,y}$ couples to the reflective modulator, a portion of the field is transmitted into the cavity through mirror 1 and the rest is reflected back to the optical fiber. Inside the cavity the field travels back and forth between the mirrors. The fields in forward and backward directions are represented as $\boldsymbol{E}_{\omega,+}^{x,y}$ and $\boldsymbol{E}_{\omega,-}^{x,y}$, respectively. At mirror 1 and mirror 2, some parts of the travelling fields are reflected back to the gain medium, and the rest are transmitted. The total output field $\boldsymbol{E}_{\omega,\mathrm{out}}^{x,y}$ produced by the reflective modulator is a sum of the output field from the cavity and the reflection of the input field:

$$\boldsymbol{E}_{\omega,\mathrm{out}}^{x,y} = \sqrt{\boldsymbol{R}_1^{x,y}}\eta_c^{x,y}\boldsymbol{E}_{\omega,in}^{x,y} + \sqrt{(\mathbf{1}-\boldsymbol{R}_1^{x,y})\eta_c^{x,y}}\boldsymbol{E}_{\omega,-}^{x,y}(\mathbf{0}) \tag{5}$$

where $\boldsymbol{R}_1^{x,y}$ and $\eta_c^{x,y}$ are the reflectivity of mirror 1 and the coupling efficiency. The backward travelling field at mirror 1 can be represented as

$$\begin{aligned}\boldsymbol{E}_{\omega,-}^{x}(\mathbf{0}) &= \sqrt{\boldsymbol{R}_2^{x}}\boldsymbol{E}_{\omega,+}^{x}(\mathbf{0})\exp\left[\boldsymbol{g}_{\mathrm{avg}} + \boldsymbol{i2\omega nL/c}\right]\\ \boldsymbol{E}_{\omega,-}^{y}(\mathbf{0}) &= \sqrt{\boldsymbol{R}_2^{y}}\boldsymbol{E}_{\omega,+}^{y}(\mathbf{0})\exp\left[\boldsymbol{g}_{\mathrm{avg}}\boldsymbol{C}_{\mathrm{pol}} + \boldsymbol{i2\omega nL/c}\right]\end{aligned} \tag{6}$$

where $\boldsymbol{R}_2^{x,y}, \boldsymbol{g}_{\mathrm{avg}}, \boldsymbol{C}_{\mathrm{pol}}, \boldsymbol{n}, \boldsymbol{L}$, and c are the reflectivity of mirror 2, the average round-trip gain for the field, the polarization-dependent gain (PDG) coefficient, the group index of the gain medium, the cavity length, and the speed of light, respectively. The field in the forward direction at mirror 1 can be expressed as the sum of the reflection of $\boldsymbol{E}_{\omega,-}^{x,y}(\mathbf{0})$ and the injected field:

$$\boldsymbol{E}_{\omega,+}^{x,y}(\mathbf{0}) = \sqrt{(\mathbf{1}-\boldsymbol{R}_1^{x,y})\eta_c^{x,y}}\boldsymbol{E}_{\omega,\mathrm{in}}^{x,y} + \sqrt{\boldsymbol{R}_1^{x,y}}\boldsymbol{E}_{\omega,-}^{x,y}(\mathbf{0}). \tag{7}$$

Given that the input field is a spectrum-sliced ASE, the initially injected field (at $\boldsymbol{t}=\mathbf{0}$ and $\boldsymbol{z}=\mathbf{0}$) can be expressed in the frequency domain as

$$\boldsymbol{E}_{\omega,+}^{x,y}(\mathbf{0})\big|_{t=0} = \sqrt{(\mathbf{1}-\boldsymbol{R}_1^{x,y})\eta_c^{x,y}}\;\boldsymbol{E}_{SS\mathrm{ASE}}^{x,y}(\omega)\big|_{t=0}. \tag{8}$$

From (6)–(8), the electric field after the kth round trip (at $\boldsymbol{t}=\boldsymbol{k}\tau_R$ and $\boldsymbol{z}=\mathbf{0}$) can be obtained as shown in (9). Here, $\boldsymbol{\tau}_R, \boldsymbol{\alpha}$, and $\boldsymbol{G}_m$ are the round-trip time, the linewidth enhancement factor, and the gain envelope, respectively. The gain envelope

was assumed to have the Lorentzian profile:

$$\begin{aligned}\boldsymbol{E}^{x}_{\omega,+}(\mathbf{0})\big|_{k\tau_R} &= \sqrt{(\mathbf{1}-\boldsymbol{R}^{x}_{1})\eta^{x}_{c}}\;\boldsymbol{E}^{x}_{\mathrm{SSASE}}(\omega)|_{k\tau_R}\\ &\quad+\boldsymbol{E}^{x}_{\omega,+}(\mathbf{0})\;|_{(k-1)\tau_R}\;\sqrt{\boldsymbol{R}^{x}_{1}\boldsymbol{R}^{x}_{2}}\\ &\quad\times\exp\left[\boldsymbol{g}_{\mathrm{avg}}\;|_{k\tau_R}\;(\mathbf{1}-\boldsymbol{i}\alpha)\boldsymbol{G}_{m}+\boldsymbol{i}2\boldsymbol{\omega}\boldsymbol{n}\boldsymbol{L}/\boldsymbol{c}\right]\\ \boldsymbol{E}^{y}_{\omega,+}(\mathbf{0})\big|_{k\tau_R} &= \sqrt{(\mathbf{1}-\boldsymbol{R}^{y}_{1})\eta^{y}_{c}}\;\boldsymbol{E}^{y}_{\mathrm{SSASE}}(\omega)|_{k\tau_R}\\ &\quad+\boldsymbol{E}^{y}_{\omega,+}(\mathbf{0})\big|_{(k-1)\tau_R}\;\sqrt{\boldsymbol{R}^{y}_{1}\boldsymbol{R}^{y}_{2}}\\ &\quad\times\exp\left[\boldsymbol{g}_{\mathrm{avg}}\big|_{k\tau_R}\;\boldsymbol{C}_{\mathrm{pol}}(\mathbf{1}-\boldsymbol{i}\alpha)\boldsymbol{G}_{m}\right.\\ &\qquad\left.+\boldsymbol{i}2\boldsymbol{\omega}\boldsymbol{n}\boldsymbol{L}/\boldsymbol{c}\right] \qquad (9)\end{aligned}$$

$$\boldsymbol{G}_{m}=\frac{\mathbf{1}}{\mathbf{1}+(\omega-\omega_{\mathrm{peak}})^{2}/(\Delta\omega_{3\,\mathrm{dB}}/\mathbf{2})^{2}} \qquad (10)$$

$$\begin{aligned}\boldsymbol{h}(\tau+\Delta\tau)&=\boldsymbol{h}(\tau)+\Delta\tau\left[\frac{\boldsymbol{h}_{0}\boldsymbol{y}(\tau)-h(\tau)}{\tau_{c}}-\frac{|\boldsymbol{E}^{x}_{t}(\tau)|^{2}}{\tau_{c}\boldsymbol{P}^{x}_{\mathrm{sat}}}\right.\\ &\quad\times\left[\exp\left\{\boldsymbol{h}(\tau)\right\}-\mathbf{1}\right]-\frac{|\boldsymbol{E}^{y}_{t}(\tau)|^{2}}{\tau_{c}\boldsymbol{P}^{y}_{\mathrm{sat}}}\\ &\quad\left.\times\left[\exp\left\{\boldsymbol{h}(\tau)\boldsymbol{C}_{\mathrm{pol}}\right\}-\mathbf{1}\right]\right] \qquad (11)\end{aligned}$$

$$\begin{aligned}\boldsymbol{E}^{x}_{\omega,\mathrm{out}}&=\sqrt{(\mathbf{1}-\boldsymbol{R}^{x}_{1})\boldsymbol{R}^{x}_{2}\eta^{x}_{c}}\,\boldsymbol{F}^{-1}\left[\boldsymbol{E}^{x}_{\omega,+}(\mathbf{0})\big|_{N\tau_R}\right]\\ &\quad\times\exp\left[\boldsymbol{h}(\mathbf{1}-\boldsymbol{i}\alpha)\right]\\ \boldsymbol{E}^{y}_{\omega,\mathrm{out}}&=\sqrt{(\mathbf{1}-\boldsymbol{R}^{y}_{1})\boldsymbol{R}^{y}_{2}\eta^{y}_{c}}\,\boldsymbol{F}^{-1}\left[\boldsymbol{E}^{y}_{\omega,+}(\mathbf{0})\big|_{N\tau_R}\right]\\ &\quad\times\exp\left[\boldsymbol{h}(\mathbf{1}-\boldsymbol{i}\alpha)\boldsymbol{C}_{\mathrm{pol}}\right] \qquad (12)\end{aligned}$$

where ω_{peak} and $\Delta\omega_{3\,\mathrm{dB}}$ mean the center frequency and the 3 dB bandwidth of the gain envelope, respectively. To obtain the average round-trip gain ($\boldsymbol{g}_{\mathrm{avg}}$) for field $\boldsymbol{E}^{x,y}_{\omega,+}(\mathbf{0})$, the gain evolution ($\boldsymbol{h}$) in the time domain for the given intensity ($|\boldsymbol{E}^{x,y}_{t}|^{2}$) was averaged over a round trip. The gain h in the time domain was calculated as in (11), where $\Delta\tau, \boldsymbol{y}, \boldsymbol{E}_{t}(\tau), \boldsymbol{P}_{\mathrm{sat}}$, and τ_c mean the sampling period, the normalized modulation signal, the field in the time domain, the saturation power, and the carrier lifetime, respectively. Provided that y is y_1 when the modulation signal is "1" level, and y_0 when the modulation signal is "0" level. y_1 is always 1 while y_0 is less than 1. In this case, the extinction ratio is determined by the ratio of y_1 and y_0. As a result, the pump gain becomes modulated, determining the extinction ratio (ER). Finally, from (5), the output fields were obtained as given in (12). In (12), $\boldsymbol{F}^{-1}[\ ]$ stands for the inverse Fourier transform. In this case, the first term of the right-hand side in (5) was negligible compared to the second term due to the low reflectivity of mirror 1 ($\boldsymbol{R}^{x,y}_{1}$) and coupling loss. The effects of the finite reflectivity of both the front and back facets were taken into account for field evolution in a round trip. The polarization dependency of the gain is characterized as $\boldsymbol{C}_{\mathrm{pol}}$.

As explained in (9), the electric field at the kth round trip is a weighted sum of the electric fields from the initial value to the (k–1)th round trip. Therefore, the weighting factor, i.e., the round-trip net gain, should guarantee a convergence after a large number of round trips. When the reflective modulator is biased below the lasing threshold, the round-trip net gain is below unity. Thus, we do not have convergence issues. When the reflective modulator is biased above the threshold, however, it is not easy to always achieve convergence because the round-trip net gain can be close to unity for lasing. However, when we have injection light, the gain is depleted from the lasing threshold. Then, convergence is guaranteed again. In other words, the proposed model works properly for injection-seeded system, regardless of the bias condition of the reflective modulators. Note that the closed-loop gain in the results in this paper was less than 0.8 in most cases.

TABLE I
SIMULATION PARAMETERS

τ_c	Carrier lifetime	300 psec
α	Linewidth enhancement factor	4
P^x_{sat}	Saturation power (x-pol.)	0.7 mW
C_{pol}	Gain ratio (x-pol. to y-pol.)	0.92
n	Group index of gain medium	4
L	Cavity length	600 μm
R^x_1	Front-facet reflectivity (x-pol.)	0.15 %
R^y_1	Front-facet reflectivity (y-pol.)	0.1 %
R^x_2	Rear-facet reflectivity (x-pol.)	30 %
R^y_2	Rear-facet reflectivity (y-pol.)	30 %
h_0	Pump gain	21.3 dB
η^x_c	Coupling efficiency (x-pol.)	40 %
η^y_c	Coupling efficiency (y-pol.)	40 %

IV. ANALYSIS RESULTS

A. Gain Saturation

The proposed model was used to analyze the characteristics of the reflective modulator. We also performed an experiment to confirm the proposed model. In the numerical analysis, we generated 2^{17} field samples with 2^{7} pseudorandom binary sequence (PRBS). Thus, the sample number within a one-bit period was 2^{10}. Considering the 1.25 Gb/s nonreturn-to-zero (NRZ) data, the sampling period and sampling frequency were 0.78 ps and 9.78 MHz, respectively. An unpolarized F-P LD was employed for the study, and the driving current was 45 mA [5]. For the optical filters, flat-top-type AWGs with 100-GHz channel spacing (bandwidth of 80 GHz or 0.64 nm) were utilized. In the simulation, the order of the super-Gaussian filter was adjusted to 1.5 to match the measured passband characteristic. The used parameters for simulation of the F-P LD are listed in Table I. Fig. 3 shows the simulated and measured optical spectra of ASE, spectrum-sliced ASE, and the output field from the F-P LD when the injection power was –10 dBm and detuning ($=\lambda_{\mathrm{Injection}}-\lambda_{\mathrm{Mode}}$) was about 0.3 nm. The simulation

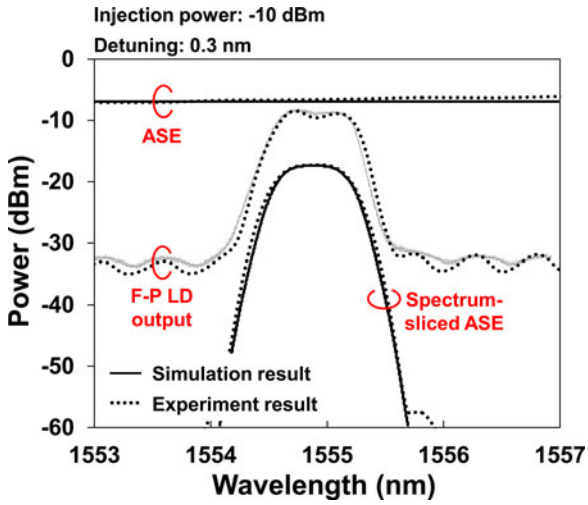

Fig. 3. Simulated and measured optical spectra of ASE, spectrum-sliced ASE, and output field of F-P LD.

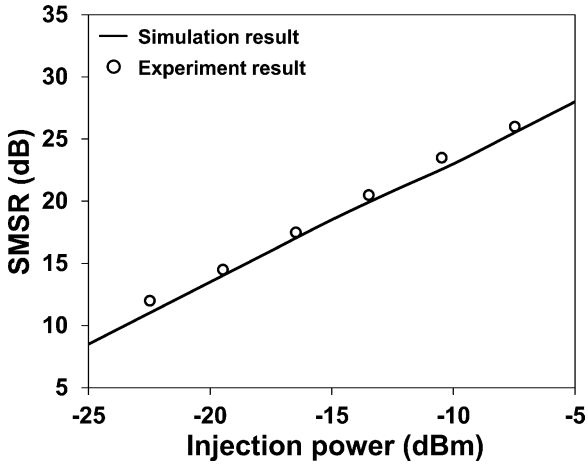

Fig. 4. SMSR as a function of injection power.

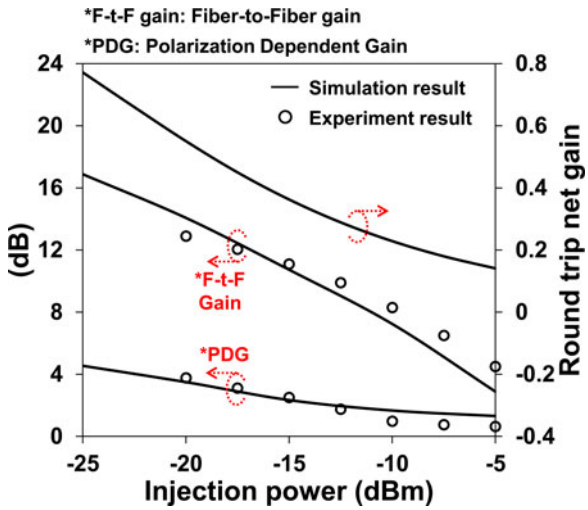

Fig. 5. Round-trip net gain, F-t-F gain, and PDG as a function of injection power.

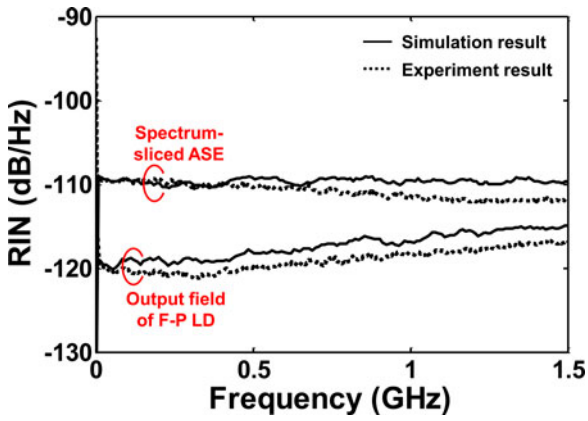

Fig. 6. RIN spectra of spectrum-sliced ASE and output field of F-P LD.

results agree well with the measured spectra. Spectral ripples were observed at the main modes and the side modes due to the effect of the cavity. As the injection power increases, the side-mode suppression ratio (SMSR) increases as can be seen in Fig. 4 since the injection effect increases.

The calculated and/or the measured round-trip net gain, fiber-to-fiber gain (F-t-F gain), and corresponding PDG are shown in Fig. 5. These values were calculated and/or measured at the output of the F-P LD. To obtain the meaningful signal light only, the side modes and/or background emission were filtered out by an optical bandpass filter (OBPF) of which the bandwidth was about 160% of the AWG bandwidth. The filter response of the OBPF was an ideal flat-top profile with a very sharp roll-off at the filter edges.

The round-trip net gain was maintained below 0.8 above –25 dBm injection power, meeting the convergence condition for the weighting factor. Also, as expected, it decreased when the injection power increased due to the carrier depletion in the gain medium. Consequently, F-t-F gain and PDG decreased [5].

B. RIN Suppression

The RIN of the injected field is suppressed by the gain saturation effect shown in Fig. 5. Fig. 6 shows the RIN spectra of the spectrum-sliced ASE and the output field of the F-P LD. The injection power and wavelength detuning were –10 dBm and 0.3 nm, respectively. With the flat-top AWG with 100-GHz channel spacing, the input RIN was about –110 dB/Hz [17]. The RIN suppression was about 10 dB at dc and 5 dB at 1.5 GHz. The RIN difference between the simulation and experiment in the high-frequency region comes from the frequency response of the avalanche photodiode (APD) used.

We measured and calculated the average RIN as a function of the injection power, and detuning as shown in Fig. 7. The average range was from dc to 750 MHz considering 1.25 Gb/s transmission. At a low injection power, the F-P LD operation is similar to that of laser, and the RIN value outweighs the input RIN (–110 dB/Hz) because the mode partition noise is generated as a result of the main-mode filtering by the OBPF. As we increase the injection power, the RIN decreases (or the noise suppression increases). At injection power levels higher than –20 dBm, the RIN values decrease below –110 dB/Hz.

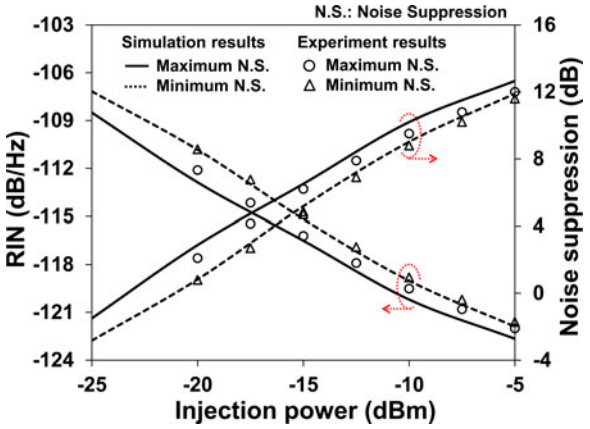

Fig. 7. Noise suppression and corresponding RIN values as a function of the injection power and detuning.

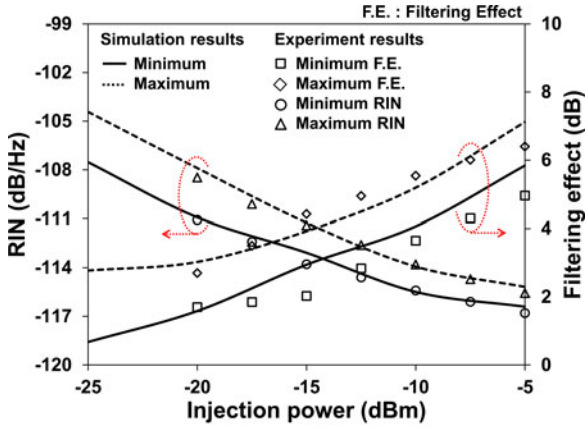

Fig. 8. Filtering effect and corresponding RIN values at receiver as a function of the ASE injection power.

The gain-saturated F-P LD leads to interactions between various spectral components of the input ASE light. As a result, the output light becomes nonthermal. To be specific, in response to the variation in the intensity of a single spectral component, the gain is inversely modulated to suppress the intensity fluctuation. Therefore, all the other spectral components are modulated inversely to the single spectral component. This phenomenon occurs to all of the spectral components, leading to anticorrelation between various spectral components of the output light [11]. The maximum and minimum noise suppressions are determined according to the wavelength detuning. When the input light is injected between two modes of the F-P LD, the noise suppression becomes maximal because the optical spectrum broadens due to the mode features. On the contrary, the peak injection (zero detuning) minimizes the noise suppression. This is valid for the comparable mode spacing of the F-P LD to the bandwidth of the spectrum-sliced ASE.

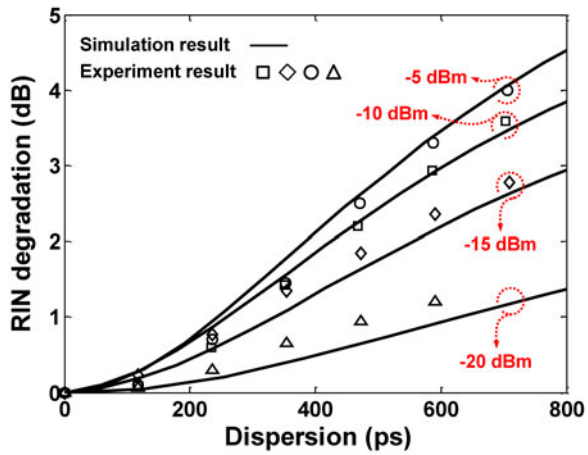

Fig. 9. RIN increases by the dispersion (phase decorrelation).

C. RIN Degradation

The noise-suppressed optical output from the F-P LD passes through two AWGs and optical fibers to get to the receiver regardless of the transmission direction as shown in Fig. 1. When the optical signal goes through the AWG, some spectral components are filtered out, which results in the breaking of the anticorrelation between the spectral components as well as a decrease in the spectral width. Consequently, the intensity fluctuation, concretely the RIN, increases again, and this is called the filtering effect [12].

Based on the proposed model, we investigated the RIN degradation caused by the filtering effect in the ASE injection-seeded DWDM system. As shown in Fig. 8, the RIN increment due to the filtering effect increases as the ASE injection power increases. The details of the filtering effect depend on the output spectral shape of the F-P LD. The spectral shape is a function of many parameters, such as the wavelength detuning, the injection power, and mode properties or cavity parameters of the reflective modulator. It is obvious that the RIN degradation increases as more spectral components are filtered out. For example, if mode peaks remain within the AWG passband, the filtering effect is small. However, if one of the mode peaks is located at the edge of the AWG passband, the power loss due to the filtering effect increases and the RIN increment becomes larger. In addition, there is mode partition noise when the injection power is low.

As well as the degradation of the signal quality due to the filtering effect, the RIN is also increased by chromatic dispersion when the optical signal propagates along the optical fibers (feeder and drop fibers). The dispersion gives rise to the breaking of the anticorrelation due to the different propagation velocity (or phase) of each spectral component. This is called phase decorrelation [10]–[12]. Phase decorrelation makes the noise of "1" level signal increased in priority at high frequencies. This was investigated through simulation and experiment, as shown in Fig. 9. The bandwidth of the output from the F-P LD after passing through the OBPF was about 85.5 GHz (0.69 nm), and the dispersion value of the fiber was 17 ps/(nm·km). The RIN of the transmitted optical signal deteriorates as the cumulative dispersion increases, and the scale of the degradation also increases as the injection power increases.

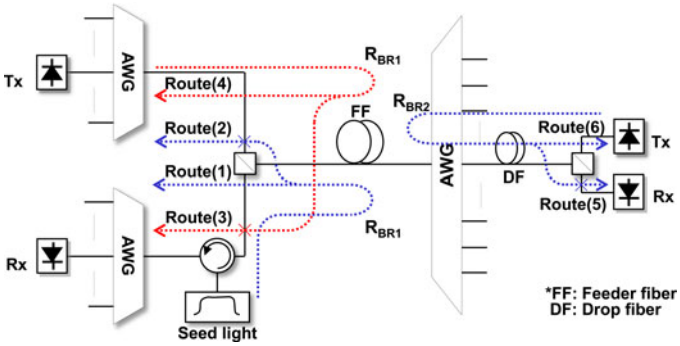

Fig. 10. Back reflections in the injection-seeded DWDM system.

D. Back Reflections

In the DWDM system based on ASE injection seeding, there is intrachannel crosstalk (or in-band crosstalk) that generates interference between signal light and the back-reflected light in most cases. This is one of the most serious impairments because the injection light and signal light occupy the same wavelength and propagate in opposite directions. The back reflections, which have various origins, are generated by Rayleigh back scattering (RBS) in the optical fiber and some imperfect connections at optical connectors or splicing points. The various routes are shown in Fig. 10. Among them, back-reflected light in routes 2, 3, and 5 is suppressed by separating the wavelength band of up- and downstream with DWDM filters. The most significant ones are routes 1 and 6 in the upstream transmission and route 4 in the downstream transmission.

In the case of route 1, a portion $(\boldsymbol{R}_{\mathrm{BR-I}})$ of the seed light is reflected back mainly due to the RBS. We call this back reflection-I (BR-I) [13], [14]. In addition, in the case of route 6, the modulated optical output from the reflective modulator is reflected back in the optical path $(\boldsymbol{R}_{\mathrm{BR-II}})$ and added to the injection light. Accordingly, the injection light becomes modulated and its power increases; this is called back reflection-II (BR-II) [13], [14]. Because of BR-II, the output signal of the F-P LD has four levels.

We investigated the reflection effect on the 1.25 Gb/s upstream NRZ signal transmission based on the proposed model. The RIN of the optical signal without back reflections was –110 dB/Hz. The crosstalk levels causing the power penalty of 1 dB at the bit error rate (BER) of 10^{-12} were about –10 and –3 dB in case of BR-I and II, respectively, as shown in Fig. 11. In the case of BR-II, the modulated injection light is suppressed through the gain saturation of the reflective modulator. Note that the increased injection power due to BR-II makes the gain of the reflective modulator more saturated. In addition, the injection current that signifies "0" level with the ER suppresses the modulated injection light. As a result, the effect of BR-II on the optical signal is greatly reduced comparing to that of BR-I.

E. Reflectivity $(\boldsymbol{R}_1)$ Dependence of RIN

Front-facet reflectivity $(\boldsymbol{R}_1)$ is a key parameter of the reflective modulator that determines the RIN performance. Based on the proposed model, we investigated the $\boldsymbol{R}_1$ dependence of the

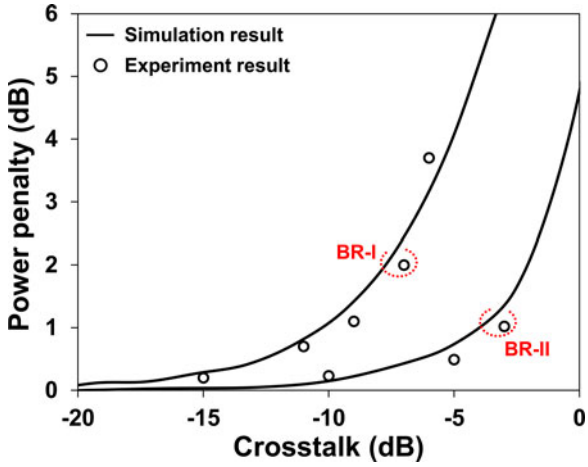

Fig. 11. Power penalties as a function of crosstalk induced by back reflections.

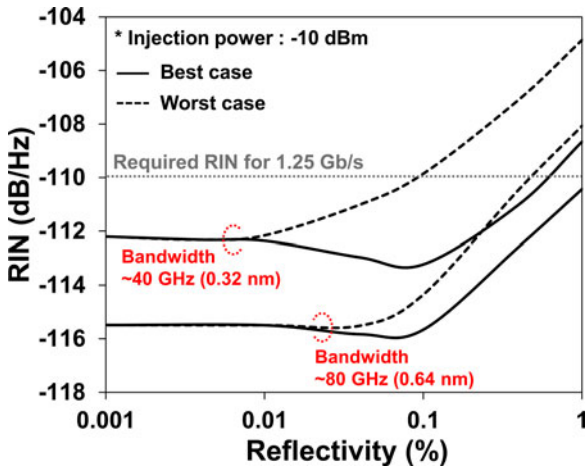

Fig. 12. $\boldsymbol{R}_1$ dependence of RIN at Rx.

received RIN in the back-to-back (B-t-B) condition through the simulation, as shown in Fig. 12. The simulation was conducted under assumption that $\boldsymbol{R}_1 = \boldsymbol{R}_1^x = \boldsymbol{R}_1^y$ and other parameters except $\boldsymbol{R}_1$ remained same as given in Table I. We also considered two different AWG bandwidths (40 and 80 GHz) to investigate the effects of injection bandwidth. The dashed and solid lines indicate the worst and best cases, respectively. $\boldsymbol{R}_1$ of 0.001% means the RSOA where the spectral ripples are diminished. In this case, there is no difference between the best and worst cases. As $\boldsymbol{R}_1$ increases, RIN difference arises, resulting in the best and worst RINs. It is worth noting that the best RIN is reduced as the $\boldsymbol{R}_1$ increases, while the worst RIN is not. This is due to the fact that, in the best case, the RIN suppression is enhanced by the negative feedback at negative detuning [15]. Thus, this phenomenon can be more clearly seen when the bandwidth of injected light (40 GHz) is narrower than mode spacing (~70 GHz). However, the RIN of the best case starts to increase at around reflectivity of 0.1%. It can be explained from increases of mode partition noise. These features can be understood as general features in ASE-seeded F-P LDs. However, details are dependent on the injection power, the bandwidth of the seed light, the mode spacing, etc.

V. Conclusion

In conclusion, we proposed a theoretical model of the reflective modulator for the seeded DWDM system based on ASE light. The model was based on the travelling-wave amplifier model. The boundary conditions were imposed by updating the field at every round trip. Using this model, the performance of the reflective modulator was analyzed in terms of SMSR, gain, and RIN suppression as functions of injection power and/or detuning is a 100-GHz channel spacing system. Based on the results, RIN increments due to the filtering effect and phase decorrelation were investigated. Also, the back-reflection-induced penalties were examined at 1.25 Gb/s signal transmission.

References

[1] C.-H. Lee, W. V. Sorin, and B. Y. Kim, "Fiber to the home using a PON infrastructure," *J. Lightw. Technol.*, vol. 24, no. 12, pp. 4568–4583, Dec. 2006.

[2] W. R. Lee, M. Y. Park, S. H. Cho, J. Lee, C. Kim, G. Jeong, and B. W. Kim, "Bidirectional WDM-PON based on gain-saturated reflective semiconductor optical amplifiers," *IEEE Photon. Technol. Lett.*, vol. 17, no. 11, pp. 2460–2462, Nov. 2005.

[3] F. Payox, P. Chanclou, and N. Genay, "WDM-PON with colorless ONUs," presented at OFC/NFOEC, Anaheim, CA, USA, 2007, Paper OTuG5.

[4] H. D. Kim, S. G. Kang, and C. H. Lee, "A low-cost WDM source with an ASE injected Fabry-Perot semiconductor laser,," *IEEE Photon. Technol. Lett.*, vol. 12, pp. 1067–1069, Aug. 2000.

[5] H.-K. Lee, H.-S. Cho, and C.-H. Lee, "A WDM-PON with an 80 Gb/s capacity based on wavelength-locked Fabry-Perot laser diode," *Opt. Exp.*, vol. 18, no. 17, pp. 18077–18085, Aug. 2010.

[6] *Multichannel Seeded DWDM Applications with Single-Channel Optical Interfaces*, ITU-T Recommendation G.698.3, 2012.

[7] X. Cheng, Y. J. Wen, Y. Dong, Z. Xu, X. Shao, Y. Wang, and C. Lu, "Optimization of spectrum-sliced ase source for injection-locking a Fabry-Perot laser diode," *IEEE Photon. Technol. Lett.*, vol. 18, no. 18, pp. 1961–1963, Sep. 2006.

[8] M. Fujiwara, H. Suzuki, K. Iwatsuki, and M. Sugo, "Noise characteristics of signal reflected from ASE-injected FP-LD in loopback access networks," *Electron. Lett.*, vol. 42, no. 2, pp. 111–112, Jan. 2006.

[9] H.-K. Lee, J.-H. Moon, S.-G. Mun, K.-M. Choi, and C.-H. Lee, "Decision threshold control method for the optical receiver of a WDM-PON," *J. Opt. Commun. Netw.*, vol. 2, no. 6, pp. 381–388, May 2010.

[10] C.-H. Lee, J.-Y. Kim, S.-R. Mun, S.-H. Yoo, H.-Y. Rhy, and S. A. Abbas, "A standard for seeded DWDM passive networks," presented at FTTH Conf. Expo, Dallas, TX, USA, Sep. 2012, Paper PC-102.

[11] A. D. McCoy, P. Horak, B. C. Thomsen, M. Ibsen, and D. J. Richardson, "Noise suppression of incoherent light using a gain-saturated SOA: Implications for spectrum-sliced WDM systems," *J. Lightw. Technol.*, vol. 23, no. 8, pp. 2399–2409, Aug. 2005.

[12] J.-Y. Kim, S.-R. Moon, and C.-H. Lee, "Analysis of noise evolution in an injection seeded WDM-PON," presented at OptoElectron. Commun. Conf., Kaohsiung, Taiwan, Jul. 2011, Paper 5A4-1.

[13] M. Fujiwara, J. Kani, H. Suzuki, and K. Iwatsuki, "Impact of backreflection on carrier-distributed WDM single-fiber access networks," in *Proc. OptoElectron. Commun. Conf.*, Yokohama, Japan, Jul. 2004, pp. 38–39, Paper 13 B2-1.

[14] J.-H. Moon, K.-M. Choi, S.-G. Mun, and C.-H. Lee, "Effects of back-reflection in WDM-PONs based on seed light injection," *IEEE Photon. Technol. Lett.*, vol. 19, no. 24, pp. 2045–2047, Dec. 2007.

[15] K.-Y. Park and C.-H. Lee, "Noise characteristics of a wavelength-locked Fabry-Perot laser diode," *IEEE J. Quantum Electron.*, vol. 44, no. 11, pp. 995–1002, Nov. 2008.

[16] G. P. Agrawal and N. A. Olsson, "Self-phase modulation and spectral broadening of optical pulses in semiconductor laser amplifiers," *IEEE J. Quantum Electron.*, vol. 25, no. 11, pp. 2297–2306, Nov. 1989.

[17] D. M. Baney and W. V. Sorin, "Broadband frequency characterization of optical receivers using intensity noise," *Hewllet-Packard J.*, vol. 46, no. 1, pp. 6–12, Feb. 1995.

Joon-Young Kim received the B.S. degree in information and communication engineering from Inha University, Incheon, Korea, in 2007, and the Ph.D. degree from Korea Advanced Institute of Science and Technology (KAIST), Daejeon, Korea, in 2013.

He is currently a Postdoctoral Research Fellow at KAIST. His current research interests include lightwave systems and optical access networks based on the dense wavelength-division multiplexing system.

Sang-Rok Moon received the B.S. degree in physics in 2008 and the M.S. degree in electrical engineering in 2010 from Korea Advanced Institute of Science and Technology (KAIST), Daejeon, Korea, where he is currently working toward the Ph.D. degree in optical communication systems.

His current research interest includes feed-forward noise suppression in wavelength-division multiplexing–passive optical network.

Sang-Hwa Yoo received the B.S. degree in electronics from Kyungpook National University, Daegu, Korea, in 2009, and the M.S. degree in electrical engineering in 2011 from the Korea Advanced Institute of Science and Technology (KAIST), Daejeon, Korea, where he is currently working toward the Ph.D. degree in optical communication systems.

His current research interest includes lightwave systems and optical access network based on wavelength-division multiplexing–passive optical network.

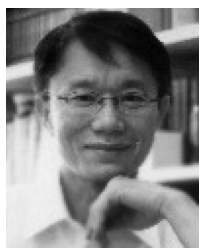

Chang-Hee Lee (M'90–SM'08–F'10) was born in 1961. He received the M.S. and Ph.D. degrees from Korea Advanced Institute of Science and Technology (KAIST), Daejeon, Korea, in 1983 and 1989, respectively.

For one year, he was a Postdoctoral Research Fellow at Bellcore (Bell Communications Research). From 1989 to 1997, he was a Senior Researcher with the Electronics and Telecommunications Research Institute. Since 1997, he has been a Professor with KAIST. He was a Technical Leader for 2.5- and 10-Gb/s optical-transmission-system development, including optical amplifiers at the Electronics and Telecommunications Research Institute. He is an author or coauthor of 170 journal and conference papers. He holds 23 U.S. patents and more than 50 additional patents are pending in the US. His current research interests include optical communications and networks.